Inorganic Chemistry
ARTICLE
pubs.acs.org/IC

Structural Studies and Electrical Properties of Cs/Al/Te/O Phases with the Pyrochlore Structure

Jun Li,[†] Theeranun Siritanon,[†] Judith K. Stalick,[‡] Arthur W. Sleight,[†] and M. A. Subramanian[*,†]

[†]Department of Chemistry, Oregon State University, Corvallis, Oregon 97331, United States
[‡]NIST Center for Neutron Research, National Institute of Standards and Technology, 100 Bureau Drive, Gaithersburg, Maryland 20899, United States

Supporting Information

ABSTRACT: A series of polycrystalline and single crystal cesium aluminum tellurates with the pyrochlore structure have been prepared and characterized. The variations in cell edge for the Cs/Al/Te/O phases range from 10.06 Å for the Al rich limit to 10.14 Å for the Te rich limit. Rietveld structural analyses based on both X-ray and neutron diffraction data were performed on 5 different compositions. Single crystals of 3 compositions were prepared and studied by X-ray diffraction. The anharmonic component of the thermal motion for Cs was small but became significant on replacing Cs with Rb. A maximum in the electrical conductivity of about 0.1 S/cm is found in the middle of this range close to the ideal composition of $CsAl_{1/3}Te_{5/3}O_6$. The conductivity is attributed to filled Te 5s states associated with Te^{4+} lying just below the conduction band based on empty Te 5s states associated with Te^{6+}. The relatively large Te^{4+} ion is compressed by the lattice, and as this compression increases the filled 5s states approach the conduction band and thereby increases conductivity.

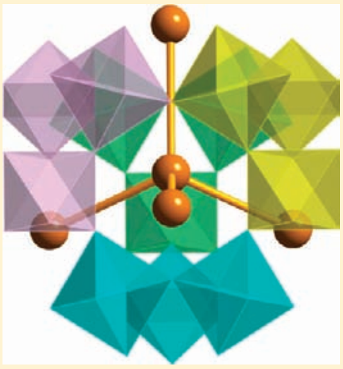

INTRODUCTION

We recently reported the first observation of electronic conductivity in mixed valent tellurium oxides.[1] These oxides have the pyrochlore structure (Figure 1) with ideal formulas such as $CsM^{3+}_{1/3}Te_{5/3}O_6$ and $CsM^{4+}_{1/2}Te_{3/2}O_6$. The oxidation state of Te in these ideal formulas is 6+. Except when M^{3+} is Tl, these phases would be expected to be electronic insulators. We had been unable to determine the deviation from the ideal stoichiometry that led to the presumed mixed valency of Te and the related electronic conductivity. A primary obstacle is our inability to dissolve these compounds to obtain a titration of the Te oxidation state. The Cs/Al/Te/O pyrochlore phase was chosen for a more intensive investigation because we found that its composition and conductivity could be varied, and the large difference in atomic numbers of Al and Te should give reliable Al/Te ratios on the octahedral site using refinements of X-ray diffraction data.

EXPERIMENTAL SECTION

Compositions of the $CsAl_xTe_{2-x}O_6$ type with x = 0.25, 0.27, 0.30, 0.33, 0.36, 0.40, 0.45, and 0.5 were prepared by solid state reaction using $CsNO_3$ (Alfa Aesar, 99.8%), TeO_2 (Aldrich, 99+%), and Al_2O_3 (Aldrich, 99.99%) as reactants. Te^{4+} is oxidized to Te^{6+} in the oxidizing atmosphere formed by the decomposition of nitrate based starting material ($CsNO_3$) and the presence of the highly electropositive Cs^+ countercation. Stoichiometric mixtures of starting materials were ground and heated twice at 600 °C for 12 h in gold crucibles with intermediate grinding. Powders were black for all values of x. Higher heating temperatures resulted in the formation of a glass. Crystals were grown using TeO_2 as a flux. A 1:1 weight ratio of a $CsAl_xTe_{2-x}O_6$ phase and TeO_2 were mixed and heated in air at 800 °C for 3 h using a gold crucible. The crucible was then cooled at 3 °C/h to 600 °C whereupon the furnace was turned off and allowed to cool to room temperature. The flux was dissolved in 1:1 aqueous HCl to free the crystals. Attempts to use a 1:4 flux ratio led to glass formation under these conditions. Examination of the "black" crystals under a microscope shows that they are dark gray and transparent. Single crystals of other $CsM_xTe_{2-x}O_6$ (M = Te, In, Ga, Ge) and $RbAl_{1/3}Te_{5/3}O_6$ pyrochlores were prepared in a similar way.[2] Powder samples of $CsM_xTe_{2-x}O_6$ (M = Ge, Mn, Zn) pyrochlores were synthesized in previous work.[1]

Our structural studies are based on powder X-ray and neutron diffraction data and on single crystal X-ray diffraction data. Neutron diffraction data for samples with nominal x values of 0.24, 0.27, 0.33, 0.38, and 0.40 were collected using the BT-1 32 detector neutron powder diffractometer at the NIST Center for Neutron Research. A Cu(311) monochromator with a 90° takeoff angle, yielding a wavelength of 1.5403(2) Å, was employed. Collimation of 15′ of arc was used before the monochromator, 20′ before the sample, and 7′ before the detectors. The samples were loaded into vanadium containers 15.8 mm in diameter and 50 mm in length. Data were collected at room temperature over a 2θ range of 3 to 168° with a step size of 0.05°. X-ray diffraction data on the same samples were collected on a Rigaku MiniFlex II diffractometer using Cu Kα radiation and a graphite monochromator. A Si internal standard was used to obtain accurate lattice parameters from the X-ray data. The neutron and XRD data were refined by the Rietveld method

Received: March 21, 2011
Published: May 09, 2011

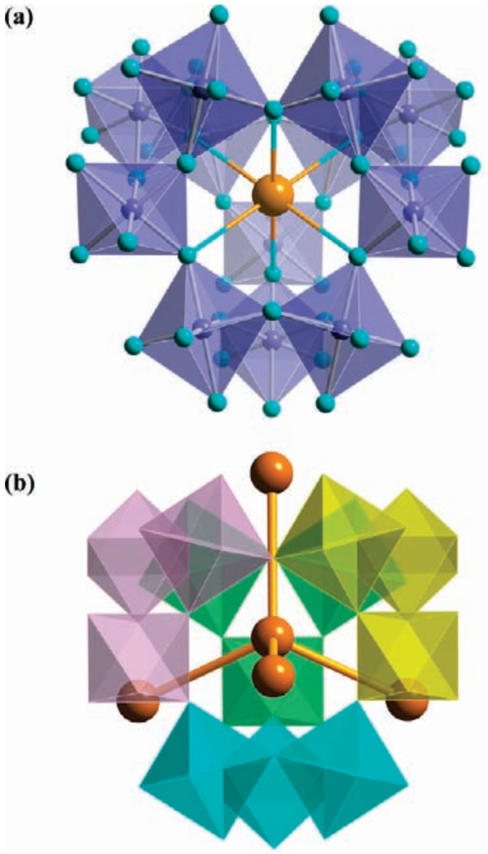

Figure 1. (a) Structure of cubic Cs(Al,Te)$_2$O$_6$ pyrochlores as a network of corner shared (Al/Te)O$_6$ octahedra (blue, 16c sites) with Cs (orange) in 8b interstitial sites. Oxygen atoms (48f) are shown in turquoise color. (b) Although the first Cs−O coordination sphere is a perfect octahedron, the symmetry of the Cs (orange, 8b sites) is actually tetrahedral. Apexes of the tetrahedron around Cs can be viewed as centers of the four colored triangles formed by corner shared (Al/Te)O$_6$ octahedra. Four neighboring Cs atoms (orange) are also tetrahedrally located around the center Cs. Different colors are used for the same (Al/Te)O$_6$ octahedra to show the tetrahedral symmetry, and the Al/Te and O atoms are not shown for clarity.

using GSAS software.[3] Single crystal X-ray diffraction data were collected using a Bruker SMART APEXII CCD system. A standard focus tube was used with an anode power of 50 kV at 30 mA. A subsequent SADABS correction was applied. The crystal structure was solved with the direct method program SHELXS and refined with full-matrix least-squares program SHELXTL.[4] Details of these single crystal structure analyses are available in cif files. These single crystal refinements confirmed the pyrochlore structure in space group $Fd\bar{3}m$. One has a choice of 4 different settings within space group $Fd\bar{3}m$. Unless otherwise indicated, in the discussion below we have placed Cs in 8b at 3/8, 3/8, 3/8, Al/Te in 16c at 0, 0, 0, and O in 48f at x, 1/8, 1/8. Atomic displacement parameters (ADPs) for Cs and Rb in single crystals of AAl$_{1/3}$Te$_{5/3}$O$_6$ (A = Rb, Cs) were refined anharmonically using the Jana software suite.[5]

Chemical analysis by electron microprobe was conducted on the single crystals. Oxidation states of tellurium were analyzed on powders of ground crystals using a ThermoScientific ESCALAB 250 X-ray Photoelectron Spectrometer with a monochromatic Al Kα source. Electrical conductivity data were obtained on sintered pellets by the four-probe method using a QD PPMS system. The contact leads used for transport measurements were thin copper wires (0.05 mm dia.) embedded on the sample by silver paste. Seebeck coefficients were determined by a static method using silver block electrodes. Reliable Seebeck coefficient values could not be obtained for samples with very low conductivities.

■ RESULTS

The results of the structural analyses are summarized in Tables 1 and 2. The cubic cell edge for phases prepared varied from 10.06 to 10.14 Å (Figure 2). The results from the neutron and XRD refinements were in good agreement, and the range of the cell edges was verified by X-ray diffraction (XRD) scans with Si as an internal standard. The value of x for a CsAl$_x$Te$_{2-x}$O$_6$ formula was determined by refining the Al/Te ratio on the 16c site. The high sensitivity of neutron data to oxygen indicated a fully occupied O site for all values of x. Because the positional parameters for oxygen are more accurate from the neutron data, these Rietveld values are used for the calculation of the interatomic distances in Table 2.

The synthesis method used for polycrystalline samples gave Al contents equal or less than as in the ideal CsAl$_{1/3}$Te$_{5/3}$O$_6$ composition. All X-ray and neutron powder diffraction patterns of these samples showed significant peak broadening and peak asymmetry. Refinement of the size and strain parameters in GSAS software indicates that the broadening is entirely due to the strain parameter. Our scanning electron microscopy (SEM) studies confirm that our crystallites are too large to produce size broadening (Figure.3). The observed broadening is not an indication of strain caused by an external stress. Instead, this is strain caused by inhomogeneities in the lattice directly related to the fact that we have cations of very different sizes on the same crystallographic sites. GSAS software treats strain, as is commonly done, requiring an equivalency of lattice expansion and lattice contraction. In such a treatment peaks remain symmetrical as they broaden. However, the physical reality is that strain can cause lattice contraction and expansion that are not equivalent, and this will produce asymmetry in the peaks as they broaden. We account for this broadening with GSAS by the addition of a second phase, but this is really just an asymmetry component of the strain (Figure.4). A more complete discussion of strain broadening of peaks may be found in the Supporting Information.

When the Al content is less than that indicated by the ideal CsAl$_{1/3}$Te$_{5/3}$O$_6$ formula, we can represent these compositions as CsAl$_{1/3-y/3}$Te$^{4+}_{y/2}$Te$^{6+}_{5/3-y/6}$O$_6$. We can also view these compositions as a solid solution between CsAl$_{1/3}$Te$_{5/3}$O$_6$ and CsTe$_2$O$_6$, which is really Cs$_2$Te^{4+}Te$^{6+}_3$O$_{12}$ with the pyrochlore structure where Te^{4+} and Te^{6+} have become ordered.[7] Given the Shannon radii[8] of 0.535 Å for Al^{3+}, 0.56 Å for Te^{6+}, and 0.97 Å for Te^{4+}, the increase in cubic cell edge is expected as y increases. It is primarily the very large Te^{4+} that causes this lattice expansion. Although Te^{4+} will be compressed by the lattice, lattice relaxation in the vicinity of Te^{4+} will cause some local lattice expansion. Furthermore, there will very likely be some clustering of Te^{4+} as a precursor to phase separation of CsTe$_2$O$_6$ from the CsAl$_{1/3}$Te$_{5/3}$O$_6$/CsTe$_2$O$_6$ solid solution. We find a solubility limit of about 30% CsTe$_2$O$_6$ in CsAl$_{1/3}$Te$_{5/3}$O$_6$. On cooling we can expect that this solubility limit would decrease, if equilibrium was achieved. Diffusion of Te^{4+} is not likely to impede phase segregation because this is really only an electron hopping process from Te to Te. However, Al diffusion will be slow and will impede phase segregation. The result may then be some clustering of Te^{4+} with no actual phase segregation. There will be lattice expansion in the areas of Te^{4+} clustering, relative to

Table 1. Structural Refinement[a] Results of Powder Neutron and X-ray (italic) and Single Crystal X-ray (bold) Data[b] for $CsAl_xTe_{2-x}O_6$

Al x[c]	Al x (refined)	Cs occupancy	cell a (Å)[d]	x(O)	χ^2/GOF	wR_p (%)
0.24	0.24(1)	0.99(1)	10.1482(1)	0.3193(1)	1.14	5.72
0.27	0.26(1)	0.99(1)	10.1417(1)	0.3194(1)	1.15	5.86
0.33	0.30(1)	0.99(1)	10.0889(1)	0.3197(1)	1.43	6.16
0.38	0.32(1)	0.99(1)	10.0890(1)	0.3196(1)	1.68	6.67
0.40	0.34(1)	0.99(1)	10.0997(1)	0.3196(1)	0.98	5.12
0.24	*0.24(1)*	*1.02(2)*	*10.1497(1)*	*0.3202(3)*	*1.84*	*9.72*
0.27	*0.26(1)*	*1.02(2)*	*10.1410(1)*	*0.3187(3)*	*1.57*	*8.97*
0.33	*0.30(1)*	*1.02(2)*	*10.0891(1)*	*0.3208(3)*	*2.58*	*11.5*
0.38	*0.32(1)*	*1.02(2)*	*10.0888(1)*	*0.3210(3)*	*2.42*	*11.2*
0.40	*0.34(1)*	*1.02(2)*	*10.0929(1)*	*0.3214(3)*	*1.94*	*9.97*
0.25	**0.38(1)**	**0.98(2)**	**10.0684(2)**	**-0.0702(4)**	**1.16**	**2.84**
0.33	**0.37(1)**	**0.98(2)**	**10.071(1)**	**-0.0697(5)**	**1.58**	**3.26**
0.45	**0.33(1)**	**0.98(2)**	**10.1035(3)**	**-0.0696(4)**	**1.40**	**3.29**

Al x	Cs[e] U_{11} (Å^2)	Al/Te U_{11} (Å^2)	Al/Te U_{12} (Å^2)	O U_{11} (Å^2)	O U_{22} (Å^2)	O U_{23} (Å^2)
0.24	0.0154(5)	0.0059(3)	−0.0003(3)	0.0079(3)	0.0135(3)	0.0044(5)
0.27	0.0175(4)	0.0073(3)	−0.0004(3)	0.0094(3)	0.0130(2)	0.0050(4)
0.33	0.0166(4)	0.0053(2)	−0.0004(3)	0.0079(3)	0.0099(2)	0.0040(4)
0.38	0.0161(5)	0.0047(3)	−0.0004(3)	0.0077(3)	0.0103(2)	0.0041(4)
0.40	0.0176(4)	0.0043(2)	0.00(2)	0.0077(3)	0.0108(2)	0.0040(4)
0.24	*0.0215(6)*	*0.0083(4)*		*0.026(3)*		
0.27	*0.0162(4)*	*0.0073(3)*		*0.026(3)*		
0.33	*0.0182(3)*	*0.0056(2)*		*0.002(1)*		
0.38	*0.0154(4)*	*0.0039(2)*		*0.002(2)*		
0.40	*0.0170(3)*	*0.0048(2)*		*0.004(1)*		
0.25	**0.0199(4)**	**0.0073(3)**	**-0.0005(1)**	**0.013(1)**	**0.014(2)**	**-0.006(2)**
0.33	**0.0157(4)**	**0.0070(3)**	**-0.0002(2)**	**0.012(1)**	**0.012(2)**	**-0.004(2)**
0.45	**0.0211(3)**	**0.0085(2)**	**-0.0004(2)**	**0.014(1)**	**0.014(2)**	**-0.007(2)**

[a] Crystal structure was refined in space group $Fd\bar{3}m$ with Cs at 8b (3/8, 3/8, 3/8), Al/Te at 16c (0, 0, 0), O at 48f (x, 1/8, 1/8) for powder neutron and XRD data; and with Cs at 8a (1/8, 1/8, 1/8), Al/Te at 16d (0, 1/2, 0), O at 48f (1/8, 5/8, 3/4-x) for single crystal XRD data. [b] XRD data of single crystals $CsAl_xTe_{2-x}O_6$ were collected at 293 K for nominal x = 0.25 and 0.45 crystals, and at 173 K for nominal x = 0.33 crystal. [c] The value of x in the first column is the nominal Al content in $CsAl_xTe_{2-x}O_6$. The same powder samples were used for neutron and X-ray data collection. [d] Standard uncertainties for powder neutron refinements, given in parentheses, do not reflect the uncertainty in the neutron wavelength. [e] Anisotropic thermal displacement parameters are expressed as $\exp[-2\pi^2 \times (U_{11}h^2a^{*2} + U_{22}k^2b^{*2} + U_{33}l^2c^{*2} + 2U_{12}hka^*b^* + 2U_{13}hla^*c^* + 2U_{23}klb^*c^*)]$; $U_{11} = U_{22} = U_{33}$, $U_{12} = U_{13} = U_{23} = 0$ for Cs; $U_{11} = U_{22} = U_{33}$, $U_{12} = U_{13} = U_{23}$ for Al/Te; $U_{22} = U_{33}$, $U_{12} = U_{13} = 0$ for O. Only isotropic thermal displacement parameters, U_{iso}, were refined for powder XRD data.

Table 2. Bond Lengths, Bond Angles, and Bond Valence Sums Calculated from Powder Neutron Structural Refinements of $CsAl_xTe_{2-x}O_6$

Al x[a]	Cs−O × 6, (Å)	Cs−O × 12, (Å)	M−O × 6, (Å)[b]	Cs,[c] BVS (Cs−O × 18)	M−O−M (deg)	O−M−O (deg)
0.24	3.1000(9)	3.6299(1)	1.9259(3)	1.40	137.16(5)	92.72(3)
0.27	3.0975(8)	3.6275(1)	1.9248(3)	1.41	137.14(4)	92.74(3)
0.33	3.0824(7)	3.6126(1)	1.9182(3)	1.48	136.98(4)	92.84(3)
0.38	3.0824(9)	3.6121(1)	1.9176(3)	1.47	137.01(5)	92.82(3)
0.40	3.0845(7)	3.6146(1)	1.9190(3)	1.45	137.01(4)	92.83(3)

[a] The value of x in the first column is the nominal Al content in $CsAl_xTe_{2-x}O_6$. [b] M stands for Al and Te that share the same 16c site. [c] Bond valence sums (BVS) were calculated using the Bond Valence Calculator.[6]

the remainder of the lattice. This will broaden peaks according to the usual strain function. This broadening decreases as y goes to 0.0 because the Te^{4+} content on 16c sites is decreasing.

Refined occupation factors indicated that most of the single crystals we prepared had an Al concentration on the 16c site greater than that indicated by the ideal $CsAl_{1/3}Te_{5/3}O_6$ formula. These samples also had smaller unit cell edges (Figure 2), consistent with the smaller size of Al^{3+} relative to Te^{6+}. Single crystals from each preparation were ground to powder for X-ray powder diffraction using a Si internal standard. The agreement between the unit cell edges determined in these two ways was very good (Figure 2). Examination of several crystals from the

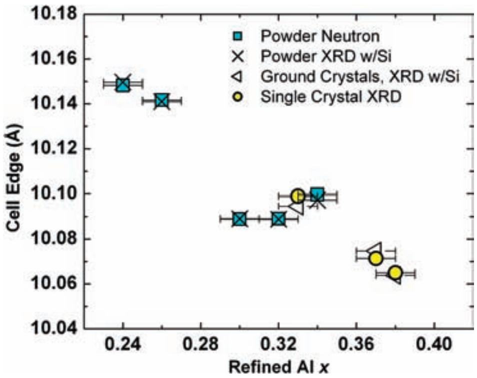

Figure 2. Variation of cell edge with refined Al content in $CsAl_xTe_{2-x}O_6$. Cell edges for ground crystals (from the same batch of the single crystal analyzed) were calculated by LeBail fit of powder XRD data with Si as an internal standard. The refined Al x values for the ground crystals were taken from the corresponding single crystal refinements. The errors in cell edge are smaller than the points (see Table 1), and error bars for x represent 1 σ.

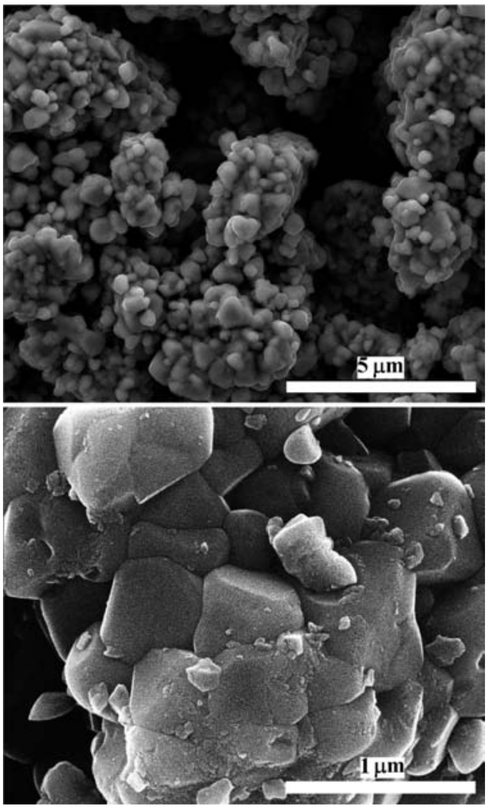

Figure 3. SEM images of $CsAl_{1/3}Te_{5/3}O_6$ (x = 0.33) powder at different magnifications.

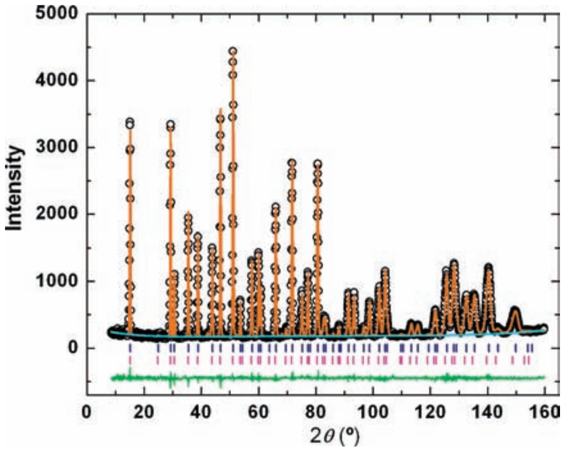

Figure 4. Rietveld refinement of neutron powder diffraction data for $CsAl_{1/3}Te_{5/3}O_6$. Applied neutron wavelength was 1.5401(2) Å (NIST BT-1). The raw data are plotted as open circles with calculated fit on top. The bottom curve shows the difference between the observed and the calculated data. Vertical bars in the first row indicate the reflection positions of cubic $CsAl_{1/3}Te_{5/3}O_6$ with cell edge 10.0889(1) Å. Vertical bars in the second row represent the asymmetric strain simulated as a second cubic phase with slightly larger cell edge 10.1140(1) Å.

same batch indicated no variation of the unit cell edge. Electron microprobe analysis on these crystals supported a slightly increased Al content relative to the ideal formula and also suggested a very small Cs deficiency. Attempts to obtain useful information on the Te^{4+}/Te^{6+} ratio from XPS were unsuccessful. The high Te^{4+} concentration we observed was presumed to be the impact of the surface. The powder diffraction peaks of the ground crystals showed no significant broadening because of size or strain. The primary issue for these samples is how to achieve charge balance for $CsAl_xTe_{2-x}O_6$ when x exceeds 1/3. None of our diffraction studies give any indication of oxygen vacancies. Thus, we must somehow add extra positive charge to compensate for this replacement of Al^{3+} for Te^{6+} on the 16c site. Various mechanisms can be proposed. All are difficult to prove at such low levels of deviation from the ideal $CsAl_{1/3}Te_{5/3}O_6$ composition. One possibility is that some cation such as Al enters the 16d site according to $CsAl_x(Al_{1/3+x}Te_{5/3-x})O_6$. The single crystal refinements suggest another possibility. The Cs occupancy for the Al rich phases consistently refines to values somewhat less than 100%, but never by more than 1σ (Table 1). A simple Cs deficiency would worsen the charge balance problem. However, we could consider that Te^{4+} has entered the cages vacated by Cs. The scattering power of Te is somewhat less than that of Cs. Furthermore, this Te^{4+} would be displaced from the center of the Cs cage. A possibility would be Te^{4+} in the 32e (x, x, x) position with x about 0.757 giving Te^{4+} three Te−O bonds of 1.98 Å on one side, a typical environment for this lone pair cation. The formula for this model would be $(Cs_{1-z}Te_z^{4+})(Al_{1/3+z}Te_{5/3-z}^{6+})O_6$ where the maximum value of z we have observed would be 0.04. This means that the maximum Te content in the proposed 32e site would be only 0.01, and this would be very difficult to detect. Detection of interstitial Al would be far more difficult because of the small atomic number of Al.

A plot of room temperature electrical resistivity versus x for $CsAl_xTe_{2-x}O_6$ phases is shown in Figure 5. With increasing Al content there is first a steady decrease in resistivity up to x = 0.33. Further increases in Al content lead to very high resistivity values. The temperature dependence of the more conducting samples (Figure 6) indicates a lower activation energy as x increases. The decrease in the absolute value of the Seebeck coefficient with increasing x is as expected for a decreasing resistivity (Figure.5). A Seebeck coefficient could not be measured in the more insulating samples. The crystals of $RbAl_xTe_{2-x}O_6$ prepared were also slightly Al rich relative to the ideal composition, and they were also found to be electrically insulating.

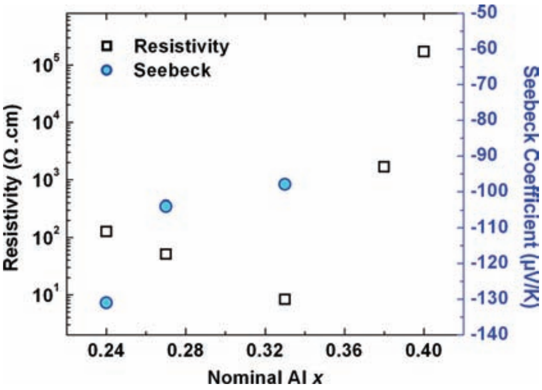

Figure 5. Variation of room temperature electrical resistivity and Seebeck coefficient versus nominal Al content in $CsAl_xTe_{2-x}O_6$ neutron samples. Uncertainties are not indicated, but are less than the point size.

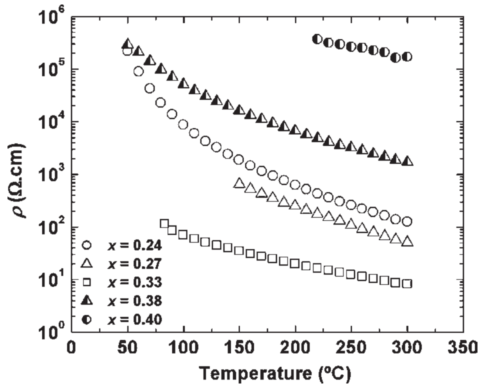

Figure 6. Resistivity of $CsAl_xTe_{2-x}O_6$ neutron samples plotted vs temperature. The values of x are nominal Al content. Uncertainties are not indicated, but are commensurate with the scatter of the data.

■ DISCUSSION

The ideal formula for the pyrochlore structure is generally considered to be $A_2M_2O_7$, but this formula may be rewritten as $A_2M_2O_6O'$ to emphasize that there are 2 different sites for oxygen with O′ being coordinated only to A cations. The space group is $Fd\bar{3}m$ with A in 16d, M in 16c, O in 48f, and O′ in 8b. The ideal pyrochlore structure may be regarded as two interpenetrating networks represented as $A_2O' \cdot 2MO_3$.[9] The network of corner-sharing $MO_{6/2}$ octahedra is the basic framework for this structure (Figure 1). The interpenetrating A_2O' network has the same structure as in Cu_2O. The O′ is sometimes missing as in the case of $AgSbO_3$.[10] Another common formulation for compounds with the pyrochlore structure is AM_2O_6.[11] Now the A cation normally occupies the 8b site. This site only becomes an acceptable site for oxygen when the 16d site is occupied by cations. The A cation in AM_2O_6 pyrochlores is normally univalent, and such pyrochlores have been evaluated for the ionic conductivity of the A^+ cation, which can be K, Rb, Cs, or Tl. Although ionic conductivity can be detected, it is very low, usually too low to detect at room temperature.[12] A typical conductivity for a CsM_2O_6 pyrochlore at 300 °C is only about 10^{-6} S/cm. The average oxidation state for M in $A^+M_2O_6$ pyrochlores is 5.5+. This site must then usually be occupied by cations of different oxidation states, which give an average oxidation state of 5.5+. One formula for such pyrochlores is $A^+M^{5+}M^{6+}O_6$. The M^{6+} cation can be W, U, or Te; the M^{5+} cation can be V, Nb, Ta, or Sb.[11] Some of these pyrochlores containing Te show a color indicative of a deviation from the ideal formula, but all are apparently electronic insulators. Other formulas for AM_2O_6 pyrochlores are $AM^{3+}_{1/3}M^{6+}_{5/3}O_6$ and $AM^{4+}_{1/2}M^{6+}_{3/2}O_6$.[11] We recently reported that some $CsM^{3+}_{1/3}Te_{5/3}O_6$ and $CsM^{4+}_{1/2}Te_{3/2}O_6$ pyrochlores could show significant electronic conductivity.[1] The electrical conductivity we observed for $CsTl_{1/3}Te_{5/3}O_6$ was not surprising because high electrical conductivity had been reported for the perovskite $BaTl_{1/2}Te_{1/2}O_3$ phase.[13] In both $CsTl_{1/3}Te_{5/3}O_6$ and $BaTl_{1/2}Te_{1/2}O_3$ the observed conductivity can be attributed to a degeneracy of the Tl 6s and Te 5s states. The other $CsM^{3+}_{1/3}Te_{5/3}O_6$ and $CsM^{4+}_{1/2}Te_{3/2}O_6$ pyrochlores show color indicative of some deviation from the ideal formulas, and this was presumed to be related to mixed valency of Te. We found significant conductivity for $CsM^{3+}_{1/3}Te_{5/3}O_6$ and $CsM^{4+}_{1/2}Te_{3/2}O_6$ pyrochlores only when M was small.[1] We have now established significant deviations from the ideal $CsM^{3+}_{1/3}Te_{5/3}O_6$ formula when M^{3+} is Al.

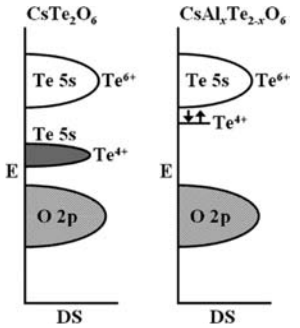

Figure 7. Schematic energy level diagrams for rhombohedral $CsTe_2O_6$ and cubic $CsAl_xTe_{2-x}O_6$ phases showing O 2p and Te 5s states only. The filled 5s states for Te^{4+} in $CsTe_2O_6$ are at lower energy than the empty 5s states because of the longer $Te^{4+}-O$ distances relative to the $Te^{6+}-O$ distances. In cubic $CsAl_xTe_{2-x}O_6$ phases the Te^{4+} states are pushed up in energy as the lattice compresses the $Te^{4+}-O$ distances with increasing x. At $x = 0.33$ the Te^{4+} donor states disappear.

Employing two different synthesis methods we have been able to vary the cubic cell edge of the Cs/Al/Te/O pyrochlore phase from 10.06 to 10.14 Å, the unit cell expanding as the Te content increases. Both synthesis methods can give a product very close to the ideal $CsAl_{1/3}Te_{5/3}O_6$ composition (Figure 2). The powder synthesis method can give Te rich phases, and the crystal synthesis method can give Al rich phases. The appropriate formula to represent this range of stoichiometry for the Cs/Al/Te/O pyrochlore phase is uncertain. For the purposes of discussion we choose to use $Cs(Al_{1/3-y/3}Te^{4+}_{y/2}Te^{6+}_{5/3-y/6})O_6$ for the Te rich phases and $(Cs_{1-z}Te^{4+}_{z})(Al_{1/3+z}Te^{6+}_{5/3-z})O_6$ for the Al rich phases. These formulas are likely only approximations to the actual situation, which appears to be very complex. The presence of Te^{4+} on the octahedral sites of the pyrochlore structure has been reported for compounds of the type $Gd_2Ti_{2-x}Te_xO_7$ where x can achieve a value as high as about 0.2.[14]

The properties of our polycrystalline samples are consistent with the $Cs(Al_{1/3-y/3}Te^{4+}_{y/2}Te^{6+}_{5/3-y/6})O_6$ formula and our previous explanation of conductivity in the $CsM^{3+}_{1/3}Te_{5/3}O_6$ and $CsM^{4+}_{1/2}Te_{3/2}O_6$ pyrochlores.[1] The conductivity is attributed to filled Te 5s states just below the conduction band (Figure 7). The energy of this level is very sensitive to the dimensions of the lattice. The filled Te 5s states are for Te^{4+}, and Te^{4+} is very large compared to Al and Te^{6+}. Thus, Te^{4+} is under compression. This compression will be relieved as the lattice expands; thus, the Te 5s state drops in energy as it is stabilized by this lattice expansion. It is for this reason that the conductivity drops with increasing y ***even though*** the number of filled Te 5s states is increasing. The temperature dependence of resistivity (Figure 6) also shows that this filled Te 5s state is dropping in energy as y increases. As y goes to zero the filled Te 5s states are lost, and there is a steep rise in resistivity. The actual point of minimum resistivity is uncertain. On the basis of nominal compositions, the minimum is very close to the ideal $CsAl_{1/3}Te_{5/3}O_6$ composition, as would be expected in this model. Refinement of the Al/Te ratio indicates that the minimum may be at an x value in $CsAl_xTe_{2-x}O_6$ of about 0.30 rather than 0.33 (Figure 2).

We represent the Al rich phases as $(Cs_{1-z}Te_z^{4+})(Al_{1/3+z}Te^{6+}_{5/3-z})O_6$. This formula is consistent with their preparation utilizing an excess of TeO_2 as a flux. There is now very little strain broadening of diffraction peaks because there is little or no Te^{4+} on the octahedral sites. We still have the filled Te 5s states shown in Figure 7, but they have moved to a lower energy because the Te^{4+} in the interstitial site is no longer under compression. These filled 5s states contribute to the observed color but not to conductivity. The pyrochlore structure is much like zeolite structures in that cations inside the cavities of the network can be highly disordered. For the $Cd_2Nb_2O_7$ and $Cd_2Ta_2O_7$ pyrochlores it was found that significant substitution for Cd could be accomplished with Mg, Mn, Fe, Co, Ni, Cu, and Zn. These cations are much too small for the Cd site and are presumed to be displaced off this site in a disordered manner.[15] In the case of the $Sn_2Nb_2O_7$ pyrochlore the Sn^{2+} is found to be displaced about 0.4 Å from the ideal position.[16] A likely site for Te^{4+} in our $(Cs_{1-z}Te_z^{4+})(Al_{1/3+z}Te^{6+}_{5/3-z})O_6$ phases is 32e because it can give 3 short Te−O distances on one side of Te, which is a normal situation for Te^{4+}. In the case of the perovskite $TeCuO_3$, the Te^{4+} has 3 short Te−O bonds on one side of Te with an average distance of 1.945 Å.[17]

Many previous studies have described Cs in the CsM_2O_6 pyrochlores as being in the 32e site, slightly displaced from the ideal 8b site. On examination of these studies we conclude there is never convincing evidence for this model. In recent refinements of the structures of $CsTi_{1/2}W_{3/2}O_6$, $CsTi_{1/4}Zr_{1/4}W_{3/2}O_6$, $CsZr_{1/2}W_{3/2}O_6$, and $CsHf_{1/2}W_{3/2}O_6$, the Cs atom was always placed in the 32e site, but the displacements of Cs from the ideal 8b site never exceeded one standard deviation.[18] Thus, in reality there is no evidence for static displacements of Cs from the 8b site. A very recent paper reexamined $CsTi_{1/2}W_{3/2}O_6$ using both X-ray and neutron powder diffraction data.[19] Again the 32e site was used for Cs. Small displacements of Cs from 8b were reported, but they were in opposite directions for the X-ray versus the neutron data. An average of the 2 refinements places Cs essentially exactly at the 8b site. Thus, again there is no evidence from these refinements for static displacements of Cs off the 8b site. We have refined the structures of 7 different CsM_2O_6 crystals using single crystal X-ray data. The cubic cell edge ranged from 10.02 to 10.32 Å for these crystals. In no case was it found that Cs in 32e rather than 8b gave a better fit to observed data. There is, however, an explanation for why the 32e site for Cs seems by some workers to be slightly preferred over 8b. There apparently has never been a refinement of any CsM_2O_6 pyrochlore using anisotropic atomic displacement parameters (ADPs) for Cs, despite the facts that Cs always has the largest U value of the three atoms in the structure and that Cs has a very high scattering power in X-ray diffraction. The reason for this is that the thermal motion of Cs is constrained to be isotropic by the symmetry of the 8b site, ***if*** one considers only the usual thermal ellipsoid model based on a harmonic potential well. However, the 8b site has tetrahedral symmetry (Figure 1) and thus an anharmonic potential well. Its thermal motion cannot be expected to be well described by the commonly used thermal ellipsoid model. Placing Cs in 32e is a way then to approximate the impact of the thermal motion of Cs in the actual anharmonic potential well. Recent studies of KOs_2O_6 with the pyrochlore structure have concluded that K is in the 8b site, but that it shows anharmonicity along the 111 direction.[20,21] However, these studies of KOs_2O_6 did not actually provide a refinement of the ADPs of the K atom, and apparently there has never been a refinement of ADPs of an A cation for a AM_2O_6 composition with the pyrochlore structure. Anharmonic thermal motion has been well studied for ZnS, ZnSe, ZnTe, and GaP.[22] Because of the high symmetry of these structures as well as the A site in the AM_2O_6 pyrochlore structure, an anharmonic refinement adds just one more parameter to the refinement for an atom at the site with tetrahedral symmetry. We find that the anharmonic component of the ADP is small for Cs but becomes obvious when Rb is substituted for Cs. This difference between the behavior of Cs and Rb might be expected because the bond valence sum for Cs is about 1.5 (Table 2) whereas the Rb value is 1.08. Thus, Cs is compressed by the lattice and more tightly held than Rb. In Figure 8 we show the result of refining the anharmonic contribution to the ADP of Rb. The resulting tetrahedron centered on the 8b site indicates that the preferred direction of the thermal motion of Rb along the 3-fold axis is toward the nearby 16d site. This might be expected because it is the empty 16d sites that provide the pathway for the ionic conductivity that is more pronounced for Rb relative to Cs because of the smaller size of Rb. The much smaller anharmonic motion of Cs appears to be in the opposite direction. This might be expected based on the 8b site potential well calculated by Pannetier.[23] More details of the anharmonic refinements are in the Supporting Information.

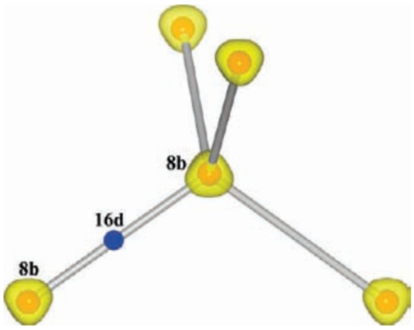

Figure 8. Neighboring Rb atoms (red) in pyrochlore $RbAl_{1/3}Te_{5/3}O_6$ are tetrahedrally arranged (lines drawn between adjacent Rb atoms to guide the eye). The Rb probability density function (PDF) cannot be described as an ellipsoid because of the tetrahedral symmetry. The application of anharmonic refinement of the PDF leads to tetrahedral-shaped probability density isosurfaces (yellow) centered in Rb atoms at 8b sites. The electron density is moving toward the empty 16d sites (blue). The lines joining the 8b sites are 3-fold axes, which extend through the 8b sites. The 32e sites lie on this 3-fold axis. Placing atoms in 32e sites close to the 8b sites approximates an anharmonic motion.

Figure 9a shows the cubic cell edge increasing as the M−O bond distance increases for all the CsM_2O_6 pyrochlores we have

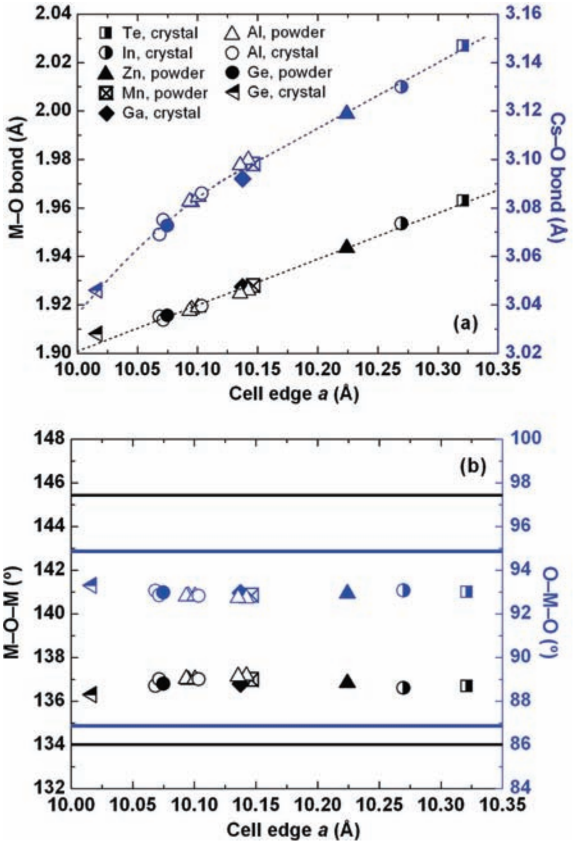

Figure 9. Bond distances (a) and angles (b) vs cell edge for all the $Cs(M,Te)_2O_6$ (M = Te, In, Zn, Mn, Ga, Al, and Ge) pyrochlore samples prepared in this and previous[1,2] work. Black and blue solid lines in (b) indicate the ranges of M−O−M and O−M−O bond angles, respectively, found for all the $A(M,M')_2O_6$ (A = K, Rb, Cs, Tl) pyrochlores.[11] Uncertainties are not indicated, but are less than the point size.

prepared and evaluated. Such dependence is expected, and this plot substantiates the reliability of our determination of the oxygen positional parameters for these phases. Figure 9a also shows that the Cs−O distance increases as the unit cell and M−O distance increase. This should not necessarily be considered expected behavior. As the M−O distance changes, one can adjust the oxygen positional parameter and the unit cell edge such that there is no change in the Cs−O distance. We start with the compound having the largest cell edge in Figure 9 to demonstrate this point. For this point we have a = 10.321 Å and x(O) = 0.3201. This gives an M−O distance of 1.963 Å and a Cs−O distance of 3.147 Å. Now consider reducing the M−O distance to 1.908 Å. This can be accomplished keeping the Cs−O distance at 3.147 Å by adjusting a to 10.155 Å and x(O) to 0.314. Instead what we find for M−O = 1.908 Å is a Cs−O distance of 3.046 Å, a cell edge of 10.017 Å, and x(O) of 0.3209. So why has the Cs−O distance changed so much when it could have remained constant? Some understanding comes from examination of the M−O−M and O−M−O bond angles (Figure 9b). These show a very small variation compared to the range known for all AM_2O_6 (A = K, Rb, Cs, Tl) compounds with the pyrochlore structure.[11] Keeping the Cs−O distance constant with decreasing M−O in the above example would cause the O−M−O angle to drop to 90.61° and the M−O−M angle to increase to 140.20°. These angles are far outside the range observed for our $Cs(M,Te)_2O_6$ pyrochlores but well within the range found for all AM_2O_6 (A = K, Rb, Cs, Tl) compounds with the pyrochlore structure, where the M−O−M angle can increase to 145.4° and the O−M−O angle can decrease to 86.9° (Figure 9b). For the CsM_2O_6 pyrochlores the framework is resisting these angle changes even though the MO_6 octahedra would become less distorted. The bond valence sum (Figure 10) for Cs (CN = 18) is above 1.0 for even the largest Cs−O distance, and only decreases slightly after adjustment is made to consider the softness of the Cs−O bond.[24] It continues to increase with the decreasing M−O distance even though this increase is not necessary. A partial explanation is that the Cs−O distance is highly compressible. The compressibility of an A−O bond increases as the oxidation state of A decreases and the size of A increases. Thus, the Cs−O bond is the most compressible of all metal−oxygen bonds.[25] This does not, however, really explain the behavior of the Cs−O distance shown in Figure 9a. The explanation may be related to the anharmonicity of the Cs thermal motion or it may be related to interstitial species other than Cs. The smooth trend for the bond valence sum of Cs in Figure 10 indicates that the change of slope for the Cs−O distance in Figure 9 for small Cs−O distance is related to the nonlinear dependence of bond valence sum and distance.

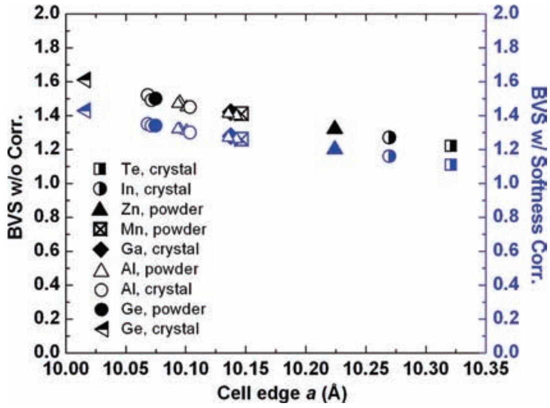

Figure 10. Bond valence sums of Cs (CN = 18, 6 short bonds and 12 long bonds) for all the $Cs(M,Te)_2O_6$ (M = Te, In, Zn, Mn, Ga, Al, and Ge) pyrochlore samples prepared in this and previous[1,2] work. BVS adjusted to the softness[24] of the Cs−O bond (blue) are slightly smaller than BVS not corrected with bond softness (black).

■ ASSOCIATED CONTENT

Ⓢ Supporting Information. Additional neutron powder diffraction patterns. More details about strain simulation and anharmonic ADPs. CIF files of the structural data of single crystals $CsM_xTe_{2-x}O_6$ (M = Te, In, Ga, Ge) and $RbAl_{1/3}Te_{5/3}O_6$ pyrochlores. This material is available free of charge via the Internet at http://pubs.acs.org.

■ AUTHOR INFORMATION

Corresponding Author

*E-mail: mas.subramanian@oregonstate.edu.

■ ACKNOWLEDGMENT

This work was supported by NSF Grant DMR 0804167. We thank Dr. Lev Zakharov for his help with single crystal work and Dr. Vaclav Petricek for his guidance in using Jana for anharmonic calculation. The identification of any commercial product or trade name does not imply endorsement or recommendation by the National Institute of Standards and Technology.

■ REFERENCES

(1) Siritanon, T.; Laurita, G.; Macaluso, R. T.; Millican, J. N.; Sleight, A. W.; Subramanian, M. A. *Chem. Mater.* **2009**, *21*, 5572–5574.

(2) Siritanon, T.; Sleight, A. W.; Subramanian, M. A. *Mater. Res. Bull.* **2011**, *86*, 820−822.

(3) Larson, A. C.; Von Dreele, R. B. Los Alamos National Laboratory Report LAUR 86-748; Los Alamos National Laboratory: Los Alamos, NM, 2004; pp 86−784. Toby, B. H. *J. Appl. Crystallogr.* **2001**, *34*, 210.

(4) Sheldrick, G. M. *SHELXTL,* Version 6.14; Bruker Analytical X-ray Instruments, Inc.: Madison, WI, 2003.

(5) Petricek, V.; Dusek, M.; Palatinus, L. *Jana 2006*, Version 10.23.2010; http://www.x-ray.fzu.cz/Jana/Jana.html, 2010.

(6) Hormillosa, C.; Healy, S.; Stephen, T.; Brown, I. D. *Bond Valence Calculator*, Version 2.0; http://www.ccp14.ac.uk/, 1993.

(7) Loopstra, B. O.; Goubitz, K. *Acta Crystallogr.* **1986**, *C42*, 520–523.

(8) Shannon, R. D. *Acta Crystallogr. A* **1976**, *32*, 751.

(9) Sleight, A. W. *Inorg. Chem.* **1968**, *7*, 1704–1708.

(10) Sleight, A. W. *Mater. Res. Bull.* **1969**, *4*, 377–380.

(11) Raveau, B. *Rev. Inorg. Chem.* **1979**, *1*, 81–112. Subramanian, M. A.; Aravamudan, G.; Subba Rao, G. V. *Prog. Solid State Chem.* **1983**, *15*, 55–143.

(12) Sleight, A. W.; Gulley, J. E.; Berzins, T. *Adv. Chem. Ser.* **1977**, *163*, 195–204.

(13) Subramanian, M. A.; Harlow, R. L.; Ramirez, A. P. *Int. J. Inorg. Mater.* **2000**, *2*, 131.

(14) Heredia, A. R.; García, M. Q.; Mazariego, J. L. P.; Escamilla, R. *J. Alloys Compd.* **2010**, *504*, 446–451.

(15) Sleight, A. W. *Mater. Res. Bull.* **1974**, *9*, 1437–1442.

(16) Birchall, T.; Sleight, A. W. *J. Solid State Chem.* **1975**, *13*, 118–130.

(17) Philippot, E.; Maurin, M. *Rev. Chim. Miner.* **1976**, *13*, 162–174.

(18) Whittle, K. R.; Lumpkin, G. R.; Ashbrook, S. E. *J. Solid State Chem.* **2006**, *179*, 512–521.

(19) Thorogood, G. J.; Saines, P. J.; Kennedy, B. J.; Withers, R. L.; Elcombe, M. M. *Mater. Res. Bull.* **2008**, *43*, 787–795.

(20) Yamaura, J. I.; Yonezawa, S.; Muraoka, Y.; Hiroi, Z. *J. Solid State Chem.* **2006**, *179*, 336–340.

(21) Hasegawa, T.; Ogita, N.; Nagao, Y.; Yamaura, J. I.; Hiroi, Z.; Udagawa, M. *Phys. C*, **2010**, in press, DOI: 10.1016/j.physc.2009.11.006.

(22) Rabadanov, M. Kh.; Loshmanov, A. A.; Shaldin, Yu.V. *Crystallogr. Rep.* **1997**, *42*, 592–662.

(23) Pannetier, J. *J. Phys. Chem. Solids* **1973**, *34*, 583–589.

(24) Adams, S. *softBV*, Version 0.96; http://kristall.uni-mki.gwdg.de/softbv/, 2004.

(25) Hazen, R. M.; Prewitt, C. T. *Am. Mineral.* **1977**, *62*, 309–315.